Reprint from

Energetics of Geological Processes

Editors

Surendra K. Saxena and Somdev Bhattacharji

Springer-Verlag
New York Heidelberg Berlin

5

S. M. SCHMID AND M. S. PATERSON

Abstract An oolitic limestone has been experimentally deformed in a wide range of temperatures (500 to 900°C) and strain rates (10^{-3} to 10^{-5}/s) involving flow stresses ranging from 30 to 2500 bars. Strain analysis on the deformed specimens reveals that, in the low stress regime (higher temperatures, lower strain rates), the relative shortening in the ooids is higher than the known shortening strain in the bulk rock, whereas at the higher stresses the ooid strain is identical with the bulk strain. The strain discrepancy at the low stresses is attributed to differences in flow stress arising mainly from differences in grain size between matrix and ooids, the fine-grained ooids being weaker in the low-stress regime. The latter effect is consistent with previous observations on marbles and Solenhofen limestone. It is argued that the low-stress regime in the experiments is representative of many geological situations in terms of the processes of deformation and hence that such strain differences between ooids and matrix could occur naturally in oolites, leading to the possibility of errors in strain analysis based on ooid shape change. The trends in ooid strain versus bulk strain are also compared with theoretical predictions based on viscous inclusion models and the significance of discrepancies discussed.

STRAIN ANALYSIS IN AN EXPERIMENTALLY DEFORMED OOLITIC LIMESTONE

occupy on the average 63% of the volume, are spaced fairly uniformly and have diameters of 0.7–1.0 mm (Fig. 1). The ooids show a remnant spherulitic structure indicated by a "dark cross" under crossed nicols (Fig. 5a) but this structure has been largely obliterated by recrystallization to ultrafine equiaxed grains of 1–2-μm diameter. Very rarely radial fibres as such survive. Most ooids also show a weak concentric structure. The mineralogical and chemical composition is very nearly uniform over both ooids and matrix, as shown by microprobe analysis of the very small traces of Mg and Fe present. There are very small, dispersed opaque impurities present in the ooids, however, possibly carbon of organic origin. These impurities are very helpful in delineating the shapes of the ooids, especially after recrystallization and grain growth has occurred at the higher temperatures.

A few ooids have formed around fossil debris. In cases where the debris particle has a high aspect ratio the ooids can deviate substantially from an initially spherical form, but such ooids are easily recognizable and very rare. They were rejected for measurements. The majority of ooids approximate fairly closely to spheres. There is a slight tendency for the longest dimension to lie parallel to bedding, giving a weak initial shape

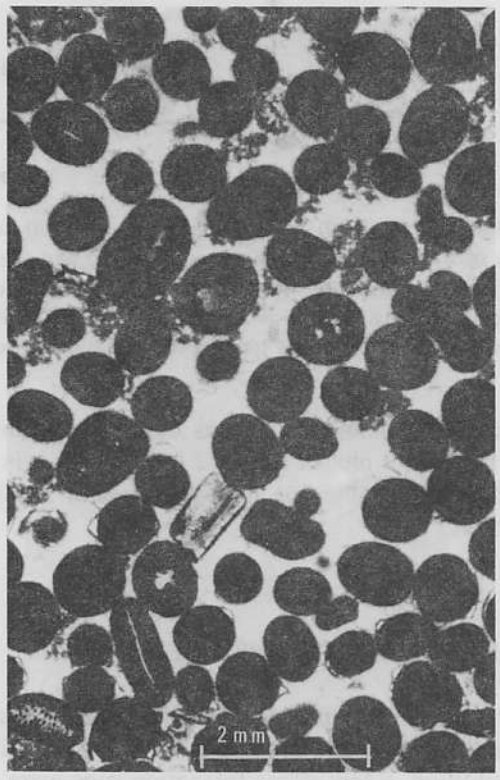

Fig. 1. Thin section of the undeformed oolite. Trace of bedding plane horizontal

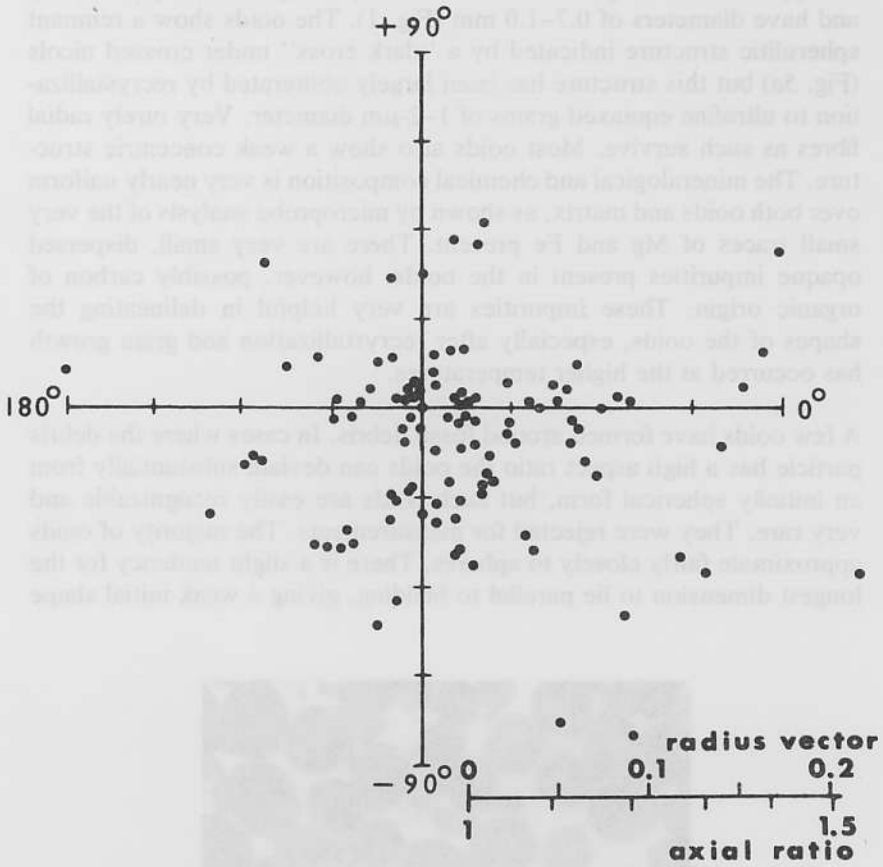

Fig. 2. Elliott plot (Elliott, 1970) of undeformed oolite (100 ooids). Half the natural logarithm of the axial ratio (radius vector scale) and the doubled angle between the long axis and the trace of the bedding plane (reference line) define a point on the graph. The distribution is nearly random and only a very slight preferential alignment of the long axis parallel to bedding is observed

anisotropy (Section 6). These properties of the initial distribution are summarized in the Elliott plot of Figure 2 from which it is seen that this oolite is particularly suitable for an experimental study. Nonoolitic debris is very rare.

3 EXPERIMENTAL DEFORMATION PROCEDURE

The specimens were, in general, deformed at constant strain rates in a high-pressure high-temperature apparatus built and described by Paterson (1970). In addition, a few stress relaxation runs were performed. It was possible to keep the temperature constant within ±5°C over the

entire length of the specimen. A sensitive internal load cell allows the detection of differential stresses as low as 10 bars.

Cores of 20-mm length and 10-mm diameter were drilled perpendicular to bedding. The specimens were sealed during deformation with 0.25-mm walled copper jackets. The temperature range of 500 to 900°C was covered, and this made it possible to cover the entire geologically interesting range of flow stresses from about 30 to 2500 bars. A standard confining pressure of 3 kbar was applied.

The stress-strain curves were derived by making the usual corrections for apparatus distortion, copper strength, and cross-sectional increase.

The amount of shortening in the specimen was obtained by measuring initial and final length with a micrometer, rather than from the load-displacement record. Thus, the nominal strain was computed at ambient conditions and is directly comparable with strains obtained by analysis of thin sections. In some of the runs at 500 to 700°C, where relatively high strains were produced at high flow stresses, thin unloading cracks parallel and, more rarely, perpendicular to the compressional axis formed. They introduce negligible errors in the strain determination, compared to other errors discussed later.

4 STRESS STRAIN RESULTS

The experiments were mostly performed at a few standard conditions in order to study the relationships between bulk, ooid and matrix strains as the amount of finite strain is increased (Table 1). Typical stress–strain curves for these conditions are plotted in Figure 3. Runs exceeding 20% shortening generally were interrupted to check the degree of homogeneity in deformation in order to avoid potential damage to the furnace. In all runs, but especially in those at high temperature, some work hardening was observed.

Generally, the degree of work hardening in materials decreases with increasing temperature. However, two reasons for this exceptional case of work hardening at high temperatures can be proposed:

(1) Progressive grain growth in the ooids occurred at high temperatures (Table 2) and increasing grain size effectively increases the flow stress if the predominant controlling mechanism is diffusional creep and/or grain boundary sliding (Schmid, 1976).
(2) It will be shown that as the strain in the specimen is increased the ratio of the strain in the matrix to the strain in the ooids increases (Fig. 9); then since the matrix is more flow resistant at high temperatures

Table 1.

Test no.	Temperature (°C)	Strain rate (per s)	Nominal bulk strain $\bar{e}_b$ (% shortening)*	Mean ooid strain $\bar{e}_{oo}$ (% shortening)*	Mean matrix strain $\bar{e}_m$ (% shortening)*
2810	500	10^{-4}	12.9	9.6	18.5
2741	500	10^{-3}	19.0	17.0	22.4
2738	500	10^{-4}	20.9	21.3	20.2
2740	500	10^{-4}	33.0	33.4	32.3
2728	600	10^{-3}	9.1	10.8	6.2
2724	600	10^{-3}	23.9	24.2	23.4
2730	600	10^{-3}	30.0	31.0	28.3
2737	700	10^{-3}	11.4	12.4	9.7
2739	700	10^{-3}	11.9	13.7	8.8
2681	700	10^{-3}	19.0	21.5	14.7
2722	700	10^{-3}	32.3	35.1	27.5
2675	800	10^{-3}	43.0	46.6	36.9
2755	800	10^{-5}	6.2	8.3	2.6
2771	800	10^{-5}	13.3	16.6	7.7
2815	800	10^{-5}	18.5	24.4	8.5
2767	800	10^{-5}	24.1	27.6	18.1
2812	800	10^{-5}	33.8	38.1	26.5
2699	800	2×10^{-5}	43.1	49.5	32.2
2756	800	10^{-5}	45.7	51.9	35.1
2817	900	10^{-5}	6.2	9.6	0.8
2779	900	10^{-5}	10.9	15.9	2.4
2765	900	10^{-5}	20.4	27.3	8.7
2789	900	10^{-5}	31.0	39.3	16.9
2799	900	10^{-5}	41.9	48.6	30.5

*Note that throughout the text and figures the engineering sign convention for strain is used, under which shortening strains are negative

because of coarser grain size, hardening is to be expected. It is not possible at this stage to evaluate the relative importance of the two factors.

In order to get additional information on the rheological behavior of the bulk rock, stress relaxation runs were performed at 600°, 700°, and 900°C. The experimental procedure and the conversion of stress rates into strain rates have been described earlier (Schmid, 1976). Figure 4 is a combined plot of constant strain rate and relaxation experiments. Stresses were determined at 10% strain in the specimen. Assuming a strain rate vs. stress relationship of the form $\dot{\epsilon} \propto \sigma^n$ a stress exponent of around $n = 5$ holds at high flow stresses, decreasing to $n < 3$ at low stresses. In terms of this stress dependence the similarities to Solenhofen limestone (Schmid, 1976) are remarkable. Marbles (Yule and Carrara) show a constant slope corresponding to $n \approx 8$ over this same region of temperature and strain rate (Heard and Raleigh, 1972). The transition

into low n value ($n < 3$) observed in Solenhofen limestone has been attributed to a change in deformation mechanism (Schmid, 1976) and there is good structural evidence (Section 5) that this is also the case in this oolite (strictly speaking in the ooids only).

A comparison of strength at various conditions between oolite, Carrara marble and Solenhofen limestone is presented in Table 2. The ratio of flow stresses at a given strain rate, corresponding to the "effective

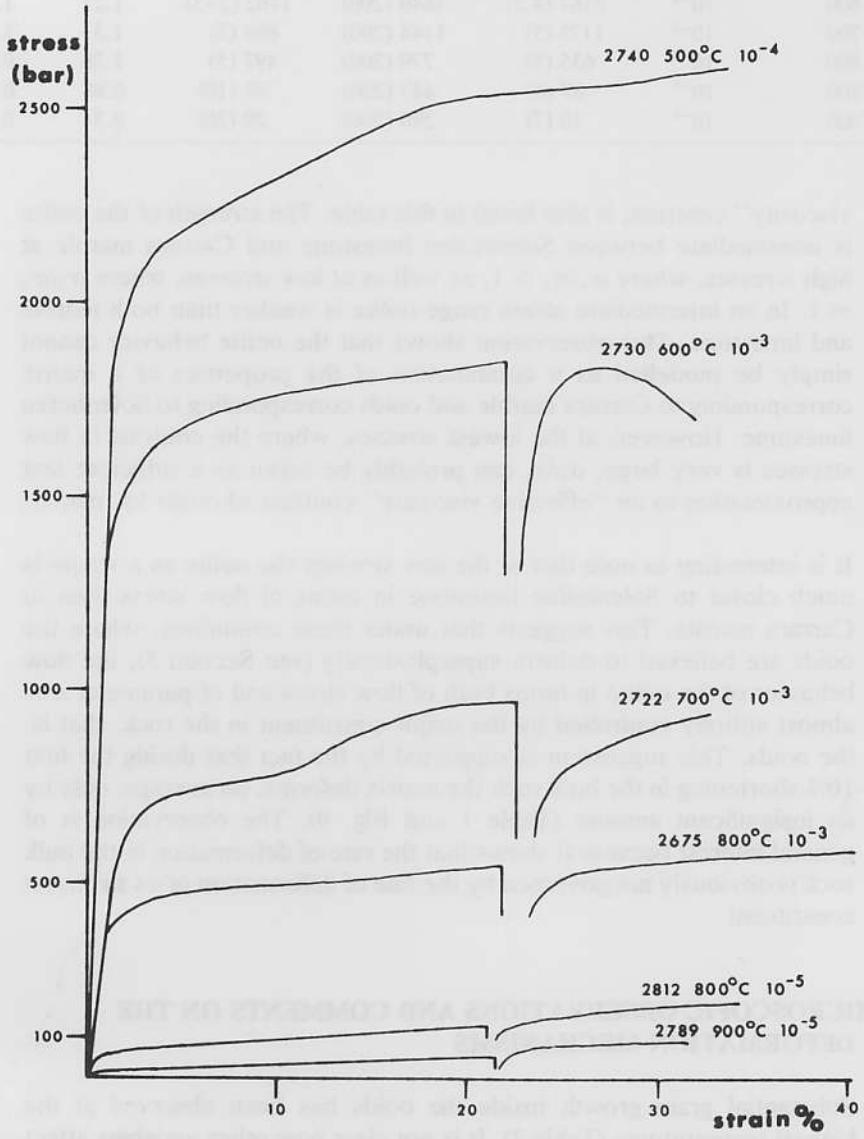

Fig. 3. Stress-strain curves for oolite

Table 2. Comparative strength and "effective viscosity" ratios in three different calcite rocks

Test conditions		Flow stress at 10% strain (bars) (Final grain size in micrometers given in parentheses)			"Effective viscosity" ratios	
Temperature (°C)	Strain rate (s)	Solenhofen σ_s	Carrara σ_c	Oolite σ_{oo}	σ_s/σ_{oo}	σ_s/σ_c
500	10^{-4}	2825 (4.5)	2060 (200)	2531 (1–2)	1.12	1.37
600	10^{-3}	2167 (4.5)	1640 (200)	1762 (2–3)	1.23	1.32
700	10^{-3}	1175 (5)	1148 (200)	860 (3)	1.37	1.02
800	10^{-3}	635 (5)	779 (200)	497 (5)	1.28	0.82
800	10^{-5}	87 (6)	447 (200)	99 (10)	0.88	0.19
900	10^{-5}	10 (7)	296 (200)	29 (20)	0.34	0.03

viscosity" contrast, is also listed in this table. The strength of the oolite is intermediate between Solenhofen limestone and Carrara marble at high stresses, where $\sigma_s/\sigma_c > 1$, as well as at low stresses, where $\sigma_s/\sigma_c \ll 1$. In an intermediate stress range oolite is weaker than both marble and limestone. This observation shows that the oolite behavior cannot simply be modelled as a combination of the properties of a matrix corresponding to Carrara marble and ooids corresponding to Solenhofen limestone. However, at the lowest stresses, where the contrast in flow stresses is very large, σ_s/σ_c can probably be taken as a sufficient first approximation to an "effective viscosity" contrast of ooids vs. matrix.

It is interesting to note that at the low stresses the oolite as a whole is much closer to Solenhofen limestone in terms of flow stress than to Carrara marble. This suggests that under these conditions, where the ooids are believed to deform superplastically (see Section 5), the flow behavior of the oolite in terms both of flow stress and of parameter n is almost entirely controlled by the major constituent in the rock, that is, the ooids. This suggestion is supported by the fact that during the first 10% shortening in the bulk rock the matrix deforms, on average, only by an insignificant amount (Table 1 and Fig. 9). The observation is of general interest because it shows that the rate of deformation in the bulk rock is obviously not governed by the rate of deformation of its strongest constituent.

5 MICROSCOPIC OBSERVATIONS AND COMMENTS ON THE DEFORMATION MECHANISMS

Substantial grain growth inside the ooids has been observed at the highest temperatures (Table 2). It is not clear how other variables affect the amount of grain growth, but the duration of time for which a

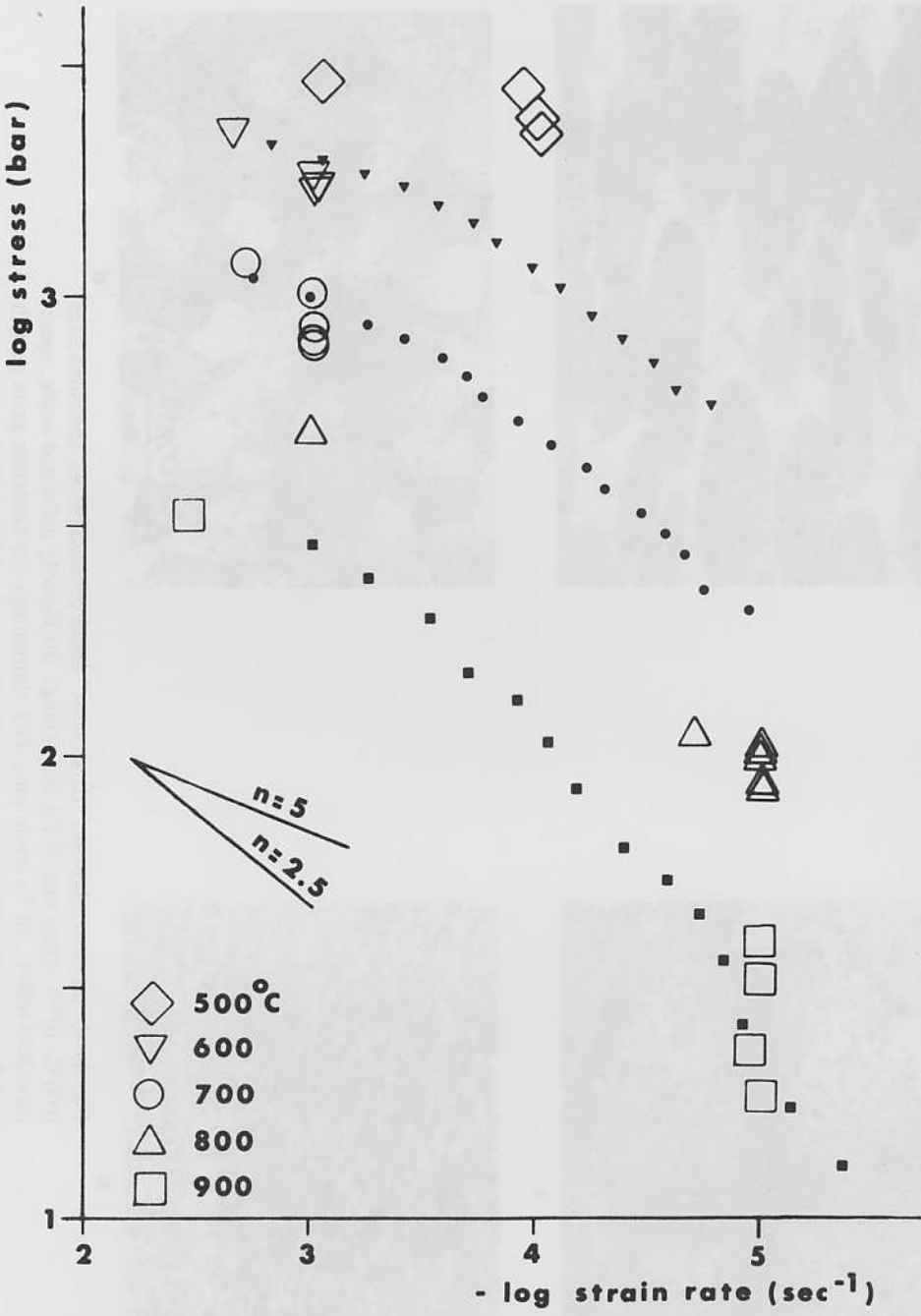

Fig. 4. Log–log plot of strain rate versus flow stress at 10% strain. *Large open symbols:* constant strain rate tests; *small closed symbols:* relaxation tests. The relaxation tests were started at 10% strain and the stress rates observed were converted into strain rates, using the known apparatus compliance

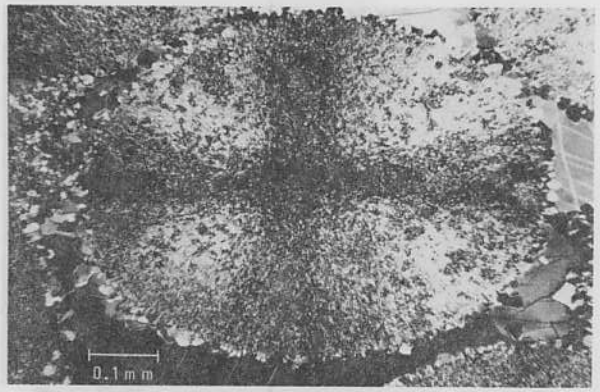

a

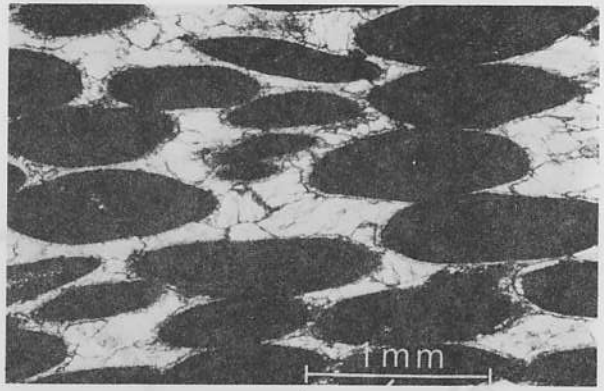

b

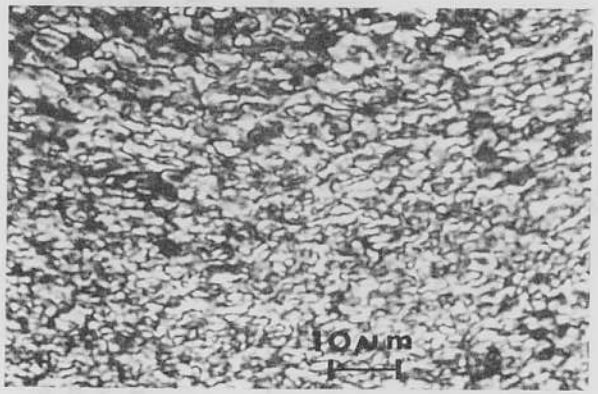

c

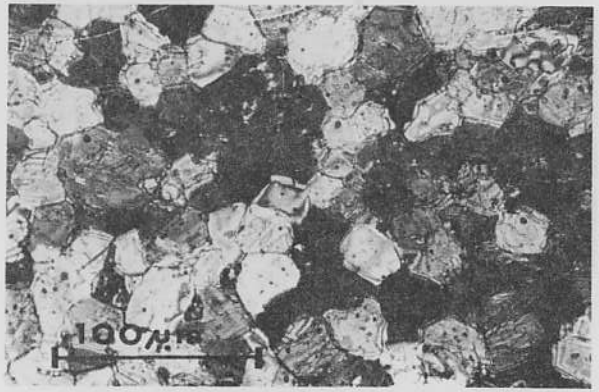

d

Fig. 5a–d. (a) Ooid, showing ''dark cross'' under crossed nicols, specimen 2728 (600°C, 10^{-3}/s strain rate, 9.1% shortening). (b) Heavily deformed oolite, specimen 2675 (800°C, 10^{-3}/s strain rate, 43% shortening). (c) Moderate grain growth and flattening of grains within an ooid of specimen 2730 (600°C, 10^{-3}/s, 30% shortening). Crossed nicols. (d) Grain growth in ooid of specimen 2799 (900°C, 10^{-5}/s, 41.9% shortening). Note absence of grain flattening in spite of the high

specimen has been at a given temperature is certainly a major factor. Differences in grain size however persist up to the highest temperatures and strains and they make it possible always to define the outlines of the deformed ooids unambiguously. These outlines are accentuated by the higher content of opaque impurities in the ooids. It is interesting that there is also a tendency, although less pronounced, for grain size reduction to occur in the matrix at the highest temperatures. This supports the idea of an equilibrium grain size being approached at any given set of conditions, although it is not clear here what parameter determines the size of this equilibrium grain size. Kohlstedt et al. (1976) suggested that a simple relationship exists between the stress and an equilibrium grain size.

The sectional shape of the deformed ooids coincides surprisingly well with that of an ellipse, even at the higher temperatures, where substantial recrystallization occurred and where a considerable effective viscosity contrast in ooids and matrix is inferred. No systematic departure from an ideally elliptical form could be found to correlate with this viscosity contrast.* This is unfortunate because the field geologist needs such an indication to decide on the reliability of his strain analysis. An alternative method of detecting a viscosity contrast is described in Section 6.

Only in specimen 2799 (900°C, 41.9% nominal strain) is the effective viscosity contrast apparently expressed structurally (Fig. 6c), and this effect in turn probably explains the strong deviation of the mean ooid strain of this sample from the trend in the remainder of the 900°C runs (Fig. 8). Figure 6c shows how virtually undeformed matrix grains are pinched into the weaker ooids. Many matrix grains in this sample show textural characteristics of porphyroclasts in a mylonite. In places boudinage of two matrix grains with "intrusion" of fine-grained oolite aggregate has been observed (Fig. 6c). Figure 6d presents evidence suggestive for grain boundary sliding between coarse matrix grains.

Intense twinning, undulatory extinction and kink band formation in the matrix grains are typical for highly strained specimens at 500° to 700°C where the matrix obviously deforms by a substantial amount (Fig. 6a). This strain is also directly recorded in substantial flattening of the matrix grains.

*Tan (1974) showed that viscosity contrast between a nucleus and its mantle within an ooid can give rise to departures from ideally ellipsoidal shape. However, the ooids in the rock used in the present study do not contain obvious nuclei and a uniform effective viscosity can be assumed within the domain of the ooid.

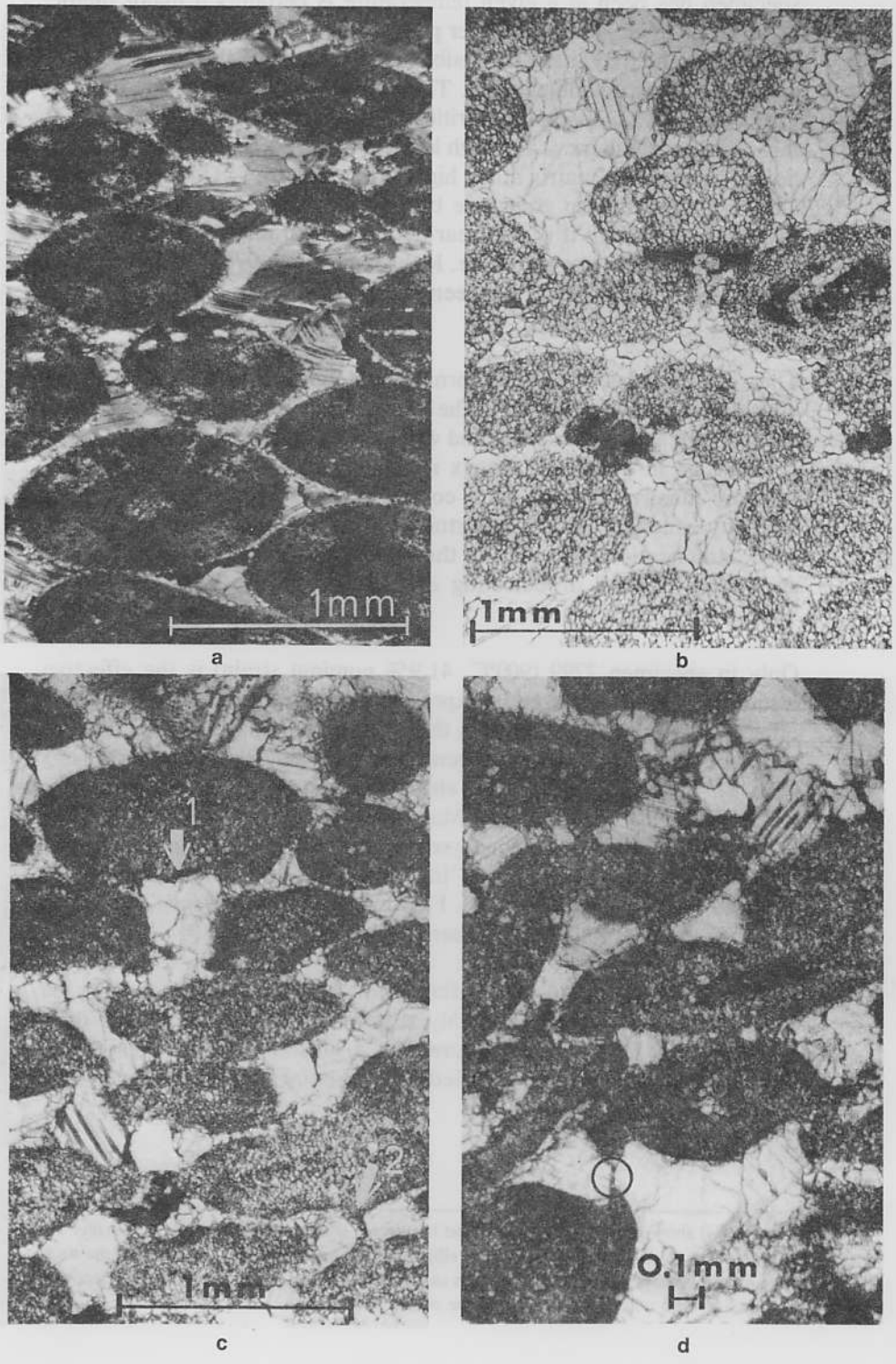
1mm
a
1mm
b
1
2
1mm
c
0.1mm
d

Clear signs of grain flattening were also found within the ooids at 500° to 700°C (Fig. 5c) but were absent at 800° and 900°C (Fig. 5d & 6b). The latter observation suggests that the predominant deformation mechanism within the ooids at the highest temperatures is grain boundary sliding, as has been proposed for Solenhofen limestone under similar conditions (Schmid, 1976, and new evidence to be published).

These microstructural observations on the matrix and ooids are consistent with similar observations on Carrara marble and Solenhofen limestone. The change in slope $n = \partial \log \dot{\epsilon} / \partial \log \sigma$ of the logarithmic stress vs. strain rate plot to values less than 3 in Solenhofen limestone and oolite, but not in marble at similar conditions, supports the idea that there is a major change in the deformation mechanism at lower stresses in fine-grained calcite aggregates within the temperature-strain rate regime studied. It is this change within the ooids that allows the substantial viscosity contrasts to build up. Similar changes in n are observed in fine-grained metals which deform superplastically and where grain boundary sliding is generally believed to be the predominant deformation mechanism (Davies et al., 1970; Edington et al., 1976).

6 STRAIN DETERMINATIONS

6.1 Strain Determination Using the Deformed Ooids

Relative shortening of the specimen parallel to its axis is reflected in the aspect ratio of an initially spherical ooid. Since the bulk deformation has rotational symmetry, such an ooid will become an oblate spheroid with axis parallel to the specimen axis. In this case, the aspect ratio as measured in a section parallel to the specimen axis is independent of whether the section is cut through the center of the ooid or not. It is assumed that there is no volume change during deformation of an ooid since bulk measurements on the specimens reveal no significant volume changes.

In this study, where the principal axes of the average bulk strain are known, the measure taken for the aspect ratio is the ratio R of the

Fig. 6a–d. (a) Heavily deformed matrix and ooids in specimen 2730 (600°C, 10^{-3}/s, 30% shortening). Note twinning and slip in matrix grains. Crossed nicols. (b) Recrystallization at 900°C (specimen 2765, 10^{-5}/s, 20.4% shortening). Note grain size reduction in matrix and grain growth in ooids. Also, note absence of flattening of individual matrix and ooid grains. (c) Marked deviation from elliptical form in ooids from run 2799 (900°C, 10^{-5}/s, 41.9% shortening). Note indentation of matrix grains into ooids (region 1) and "intrusion" of ooid aggregate between matrix grains (region 2). (d) Evidence for grain boundary sliding in specimen 2799 (encircled region). Compressional stress applied vertically in all figures

diameter of the ooid parallel to the specimen axis to the diameter normal to the axis. This measure will deviate somewhat from the true axial ratio as normally measured in strain analyses on rocks in the field where the principal axes of the bulk strain are unknown. However, for the present purpose of exploring heterogeneity of strain between ooids and matrix this measure is the most relevant quantity. It can be regarded as describing the axial ratio of an imaginary strain ellipse inscribed within the ooid; the axes of this ellipse have not rotated, on average, because of the coaxial nature of the deformation involved in the experiments. The measurements of R were made on enlarged photographs of thin sections of the deformed specimens.

In calculating the ooid strain from the measured aspect ratios account must be taken of a small initial shape anisotropy consisting of a preferential alignment of the short axes of the originally slightly non-spherical ooids perpendicular to bedding, that is, parallel to the axis of subsequent shortening. Using the same procedure as for the deformed material, the initial aspect ratios R_0 were measured on 250 ooids in an undeformed oolite specimen. The arithmetic mean of R_0 was 0.971, with a standard error of 0.008; the standard deviation of the set of individual measurements was correspondingly 0.121.

The engineering axial strain in the ooids is designated e_{oo}. If an ooid is assumed to be initially spherical, with unit diameter, and if the maximum and minimum diameters of the spheroid into which it is deformed are $(1 + e_1)$ and $(1 + e_3)$ respectively, then, from the constant volume condition $(1 + e_3)(1 + e_1)^2 = 1$, it follows that

$$e_{oo} = e_3 = R^{2/3} - 1, \tag{1}$$

where

$$R = \frac{1 + e_3}{1 + e_1}.$$

If the ooid has an initial spheroidal shape with maximum and minimum diameters $(1 + e_1)_0$ and $(1 + e_3)_0$ and if the deformation is coaxial, the constant volume condition is $(1 + e_3)_0(1 + e_1)_0^2 = (1 + e_3)(1 + e_1)^2$ and the axial strain is

$$e_{oo} = \frac{1 + e_3}{(1 + e_3)_0} - 1 = \left(\frac{R}{R_0}\right)^{2/3} - 1, \tag{2}$$

where

$$R_0 = \frac{(1 + e_3)_0}{(1 + e_1)_0}$$

We now wish to relate the strain in the ooids to the bulk strain in the oolite. In doing this in the experimental specimens, the heterogeneity in deformation arising from frictional constraint at the ends must be taken into account. We, therefore, calculate a notional or mean ooid strain $\bar{e}_{oo}$ for the whole specimen under the supposition that the matrix deforms the same as the ooids, in order to be able to compare this quantity with the nominal strain as determined from the micrometer measurements. There is a variation axially in the amount of relative shortening, with a minimum near the ends, and there is some variation radially in both amount and orientation of the principal strains due to "overflow" at the edges of the loading pistons (Fig. 7). Error due to the latter effect was minimized by not making measurements near the lateral boundaries of the specimen (in highly deformed specimens only the central half of the total area available in the thin section was used). The variation in relative shortening along the length of the specimen was allowed for by subdividing the specimen into segments of length l_i, each approximately 1 mm, and treating each segment as having uniform bulk shortening. Using Equation (2), and thus allowing for the initial anisotropy, the notional initial length $(l_i)_0$ that the ith segment would have had if it had undergone a uniform strain equal to that in the ooids within it is given by

$$(l_i)_0 = \frac{l_i}{1 + (e_{oo})_i} = l_i \left(\frac{R_0}{R_i} \right)^{2/3}$$

where the aspect ratio R_i is the arithmetic mean determined within the ith segment (usually containing between 5 and 15 ooids). The mean ooid strain for the whole specimen is given by

$$\bar{e}_{oo} = \frac{L - \sum_i (l_i)_0}{\sum_i (l_i)_0} = \frac{L}{\sum_i l_i \left(\frac{R_0}{R_i} \right)^{2/3}} - 1$$

where L is the final overall length of the specimen. The determined values of $\bar{e}_{oo}$ are listed in Table 1, expressed in engineering strain, and are plotted in Figures 8 and 9 expressed in natral strain, $\epsilon_{oo} = \ln (1 + \bar{e}_{oo})$. A total of 150 to 300 ooids was measured in each specimen.

The accuracy of the strain determination can be illustrated with reference to specimen 2765 in which the bulk deformation was homogeneous over almost the entire length (Fig. 7b). A set of 150 measurements gave an arithmetic mean of the aspect ratios of the ooids, in the homogeneous area, of 0.576, with a standard error of 0.006 and a standard deviation of individual measurements of 0.069. After taking into account the uncertainty in the initial anisotropy, quoted above, the quantity $R/R_0^{2/3}$ has a standard error of 0.006, which leads to a mean ooid strain of 29.4 ±

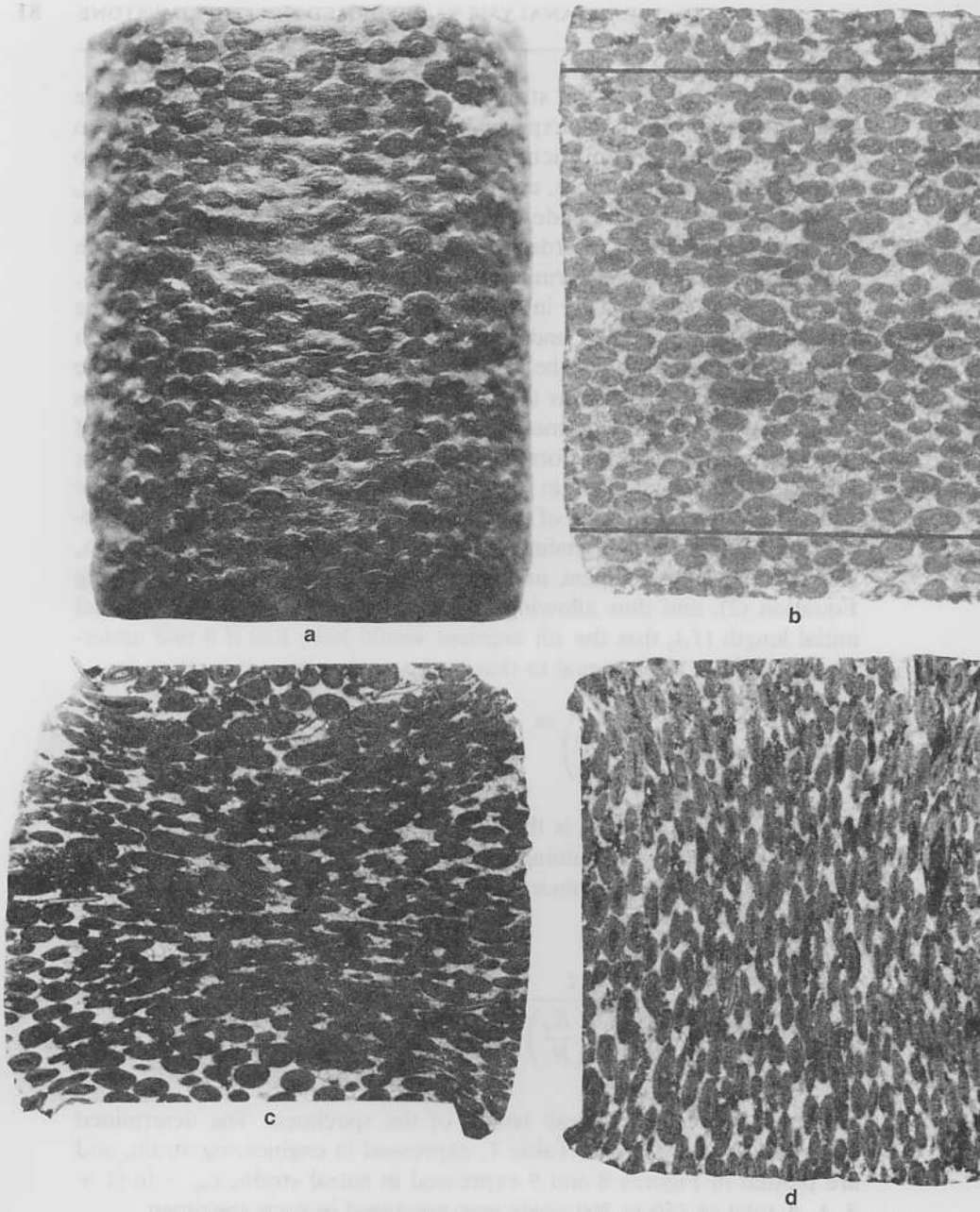

Fig. 7a–d. (a) Cylinder surface of specimen 2767 (800°C, 10^{-5}/s, 24.1% shortening). Note "squeezing" of ooids out of the cylinder surface, directly expressing the contrast in flow properties between ooids and matrix. (b) Specimen 2765 (900°C, 10^{-5}/s, 20.4% shortening), homogeneously deformed region between marker lines was used for the strain analysis reported in Section 6.2 and for statistical evaluations. (c) Very markedly inhomogeneous strain distribution within specimen 2675 (800°C, 10^{-3}/s, 43% shortening). (d) Relatively homogeneous strain distribution in specimen 2699 (800°C, 10^{-5}/s, 41.9% shortening)

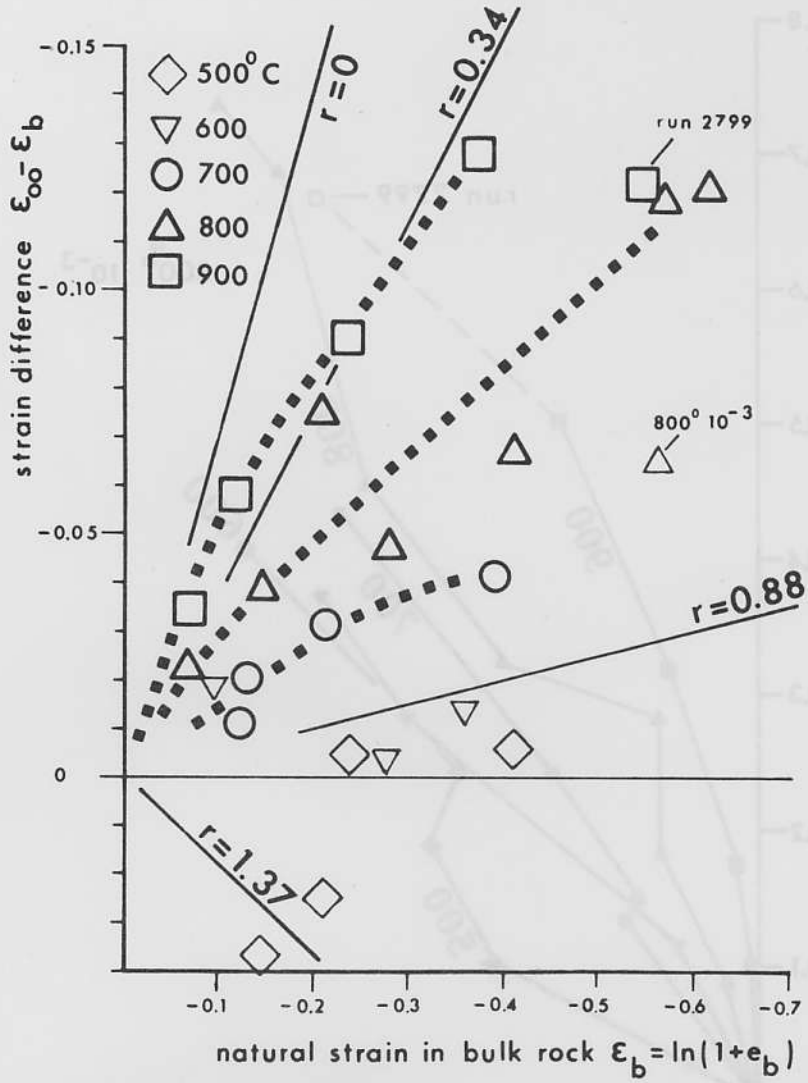

Fig. 8. Plot of the nominal bulk strain in the specimen versus the difference between the mean ooid strain and the nominal bulk strain. This strain difference corresponds to the error arising in a strain analysis based on the ooid shape, assuming that the deformation is homogeneous between ooids and matrix. Strains are plotted as natural strains $\epsilon = \ln(1 + e)$. *Broken lines:* trends at 700°, 800°, and 900°C (estimated visually); *Full lines:* theoretical predictions of the model of Bilby et al. (1975) for different viscosity contrasts r

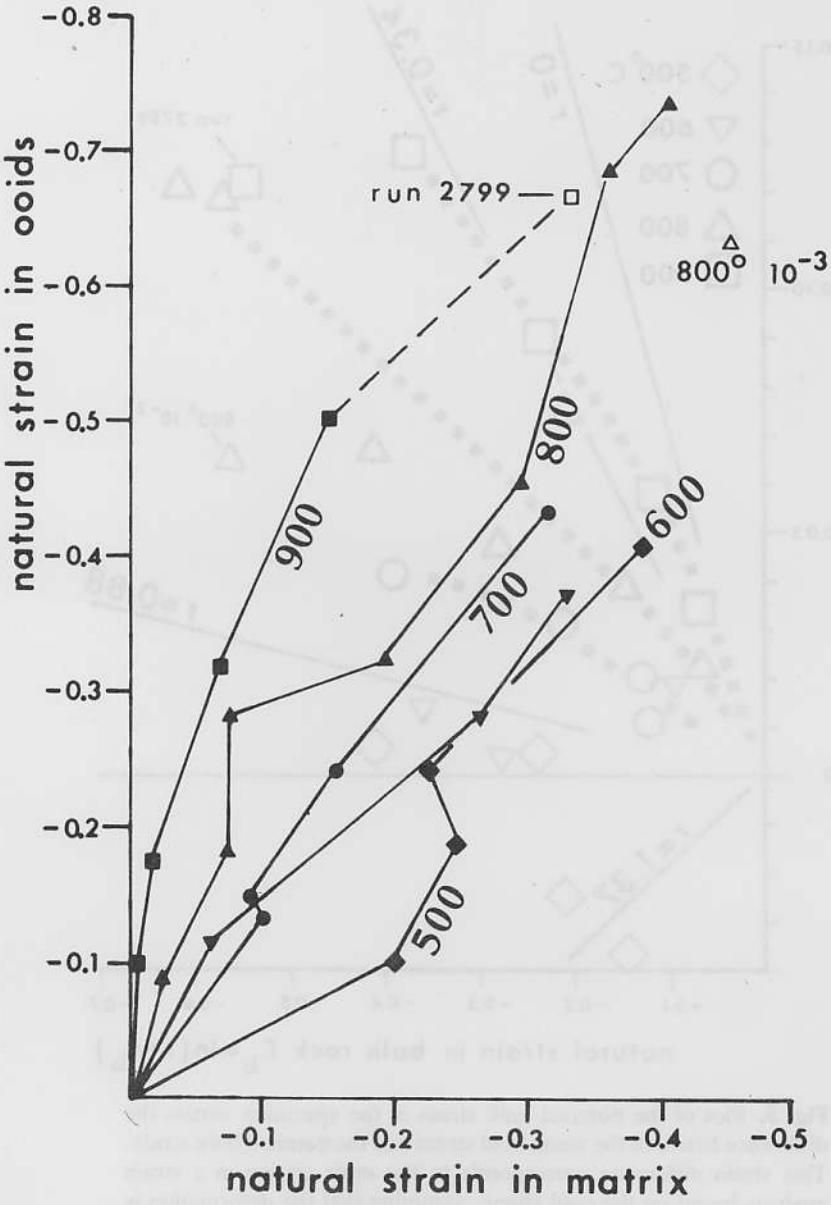

Fig. 9. Plot of the mean ooid strain versus the mean matrix strain, units of natural strain

0.6%. This precision only applies, of course, to this particular case, but it can be expected to apply approximately for all the measurements and not be greatly affected by the magnitude of the mean aspect ratio within the range of strains studied nor by the relatively small variation in strain along the specimen axis to which the summation method described above is applied.

Since the mean ooid strain $\bar{e}_{oo}$ is seen in general to be different from the nominal bulk strain $\bar{e}_b$, it is of particular interest to compare the mean ooid strain with the mean strain $\bar{e}_m$ in the matrix, calculating the latter as follows:

$$\bar{e}_m = \frac{\bar{e}_b - f_{oo}\bar{e}_{oo}}{1 - f_{oo}}$$

where f_{oo} is the volume fraction of ooids. There is clearly a variation in the relation between matrix and ooid strains as temperature and bulk strain are increased (see Table 1 and Figs. 8 and 9). Thus, while at 500°C and 600°C there is no significant departure from homogeneity between matrix and ooids, at higher temperature the concentration of deformation in the ooids, especially at relatively small strains, is well illustrated (the different behavior of specimen 2799 from the others deformed at 900°C was discussed above).

It is noteworthy that an inverse departure from homogeneity of deformation between matrix and ooids is not observed at the lowest temperatures in spite of the fact that an inversion in effective viscosity contrast between Carrara marble and Solenhofen limestone is found experimentally to occur at about 700°C for the strain rates studied here (see Table 2). This presumably is again evidence that the oolite cannot be regarded as being exactly modelled in its behavior by regarding the ooids as equivalent to Solenhofen limestone and the matrix as equivalent to Carrara marble, although such a model has qualitative validity at the higher temperature.

The existence of the large differences between $\bar{e}_{oo}$ and $\bar{e}_m$ poses a problem of strain compatibility between ooids and matrix. Clearly the local strains, especially in the matrix, must be very inhomogeneous and substantial shearing displacements must be accomodated in the matrix. However, this deformation in the matrix is readily achieved by slip and twinning within the large matrix grains.

6.2 Strain Measurement Using the Spatial Distribution of Ooids

This method, described by Ramsay (1967), is suitable for strain analysis in rocks having undergone different amounts of strain in markers and matrix and is exceptional in being, ideally, independent of contrast in flow resistance between matrix and markers. What is needed, however, is a uniform or known spatial distribution of particles (in our case, ooids) through the rock. In case of a uniform distribution, the mean distance between centers of neighboring ooids should be independent of the orientation of the line joining them, while after deformation the distance will vary from maximum to minimum values parallel respectively to the maximum and minimum principal strains. Thus, treating the problem in two dimensions for the case of rotational symmetry, the mean distance d between centers will vary with direction according to

$$d^2 = (1 + e_1)^2 \cos^2 \alpha + (1 + e_3)^2 \sin^2 \alpha \qquad (3)$$

where α is the angle between the direction of maximum principal strain, and the line joining the centers of neighboring ooids. This equation is simply a description of the axial section of the bulk strain ellipsoid.

What this describes physically is the result of bodily displacement of ooids that initially lay on a circle around a common neighbor. This bodily displacement is governed by the flow in both matrix and ooids and ideally should give a strain measure for the total rock, provided constant volume is still assumed. The bulk axial engineering strain e_b in an experimental specimen analyzed in this way is, therefore, given immediately by e_3 in Equation (3).

The practical application of this method presents two problems:

(1) Neighbors have to be defined with care, especially after high amounts of strain. Here ooids were counted as neighbors when the line connecting them does not cut through another ooid. Selection according to this criterion is, strictly speaking, influenced by the amount of inhomogeneous strain between matrix and ooids, but only to a very minor and negligible degree.
(2) The accuracy of this method is bound to be low because a very considerable scatter in d at any single α can be expected. However, if the directions of principal strain axes are known beforehand, the measurements of d can be restricted to directions parallel to those axes and an axial ratio is directly obtained. In this way, a great number of measurements can be obtained in a relatively short amount of time.

In an oolite formed by the sedimentation of spherical particles in a gravity field, the distance d between ooids touching each other in three dimensions (as is the case in many oolites including the one studied here) is likely to be large parallel to bedding and to decrease statistically towards a direction perpendicular to bedding. In order to test for such an initial anisotropy 800 measurements of d were made on an undeformed sample and plotted as a function of α, defined as the angle between the direction of d and the bedding plane in a cut perpendicular to bedding (Fig. 10). Because of the large scatter the measurements were grouped in intervals of 5° in α. The arithmetric means of these do not obviously conform closely to a relation of Equation (3) and a statistical fit has not been carried out. However, if only the 0–5° and 85–90° intervals of α are considered the initial anisotropy corresponds to a mean ratio $(1 + e_3) : (1 + e_1)$ of 0.843 with a standard error of 0.051 for the total of 90 measurements (half in each interval), or to an initial equivalent strain of $10.1 \pm 3.6\%$ using Equation (1). This value may be a useful approximation for the initial anisotropy of other oolites also, provided their sedimentary environment of formation was similar.

Because of the rather low inherent accuracy, only one deformed specimen (2765) was analyzed using this method. As noted earlier, this specimen shows homogeneous deformation over almost its entire length and it also shows a large strain difference $\bar{e}_{oo} - \bar{e}_b$. The analysis was done in order to demonstrate that the method does indeed lead to a correct measurment of strain in the bulk rock and also to assess the final accuracy of the result. This information is essential for the field geologist who wishes to estimate effective viscosity contrasts in naturally deformed oolites.

The following results apply within the region of homogeneous bulk deformation of specimen 2765 (Fig. 7b):

(1) The bulk oolite strain e'_b obtained from the spatial distribution of the ooids is 19.1 ± 5.0% (Fig. 10).
(2) The ooid strain $\bar{e}_{oo}$ obtained from analysis of the aspect ratios of the ooids is 29.4 ± 0.6%.
(3) The known bulk oolite strain $\bar{e}_b$ between the marker lines in Figure 7b is 21.9% as evaluated from micrometer measurements of the whole specimen corrected to this gauge length using the strain distibution indicated by the variation of e_{oo} along the specimen axis (this correction is small in the present specimen).

Thus, within the accuracy of the measurements, the bulk oolite strain determined from the spatial distribution of the ooids agrees with the known bulk strain, whereas a bulk strain inferred from the ooid strain under an assumption of homogeneous deformation of ooid and matrix is substantially greater. The accuracy of the former determination could be improved if more ooids were considered; in the above case, 80 measurements were available in the 0–5° interval and 35 in the 85–90° interval, defining an ellipse whose mean axial ratio had a standard error of 0.051; combining this uncertainty with an analogous value for the undeformed material (see above) led to the quoted uncertainty of ±5.0% in the determination of the bulk oolite strain (e_b').

In order to produce an alternative, graphical impression of how well the assumptions underlying this method hold, the initial variation of d as a function of α was analytically "deformed" by applying the known strain of 21.9% (Fig, 10). The "deformed" distribution is seen to agree reasonably well, within the scatter, with the measured variation of d with α in the deformed material.

7 INHOMOGENEOUS STRAIN DISTRIBUTION WITHIN A SPECIMEN

The variation in strain within the specimen is shown for two examples in Figures 7c and 7d. It is seen that the degree of inhomogeneity in bulk strain (as approximated by the ooid strain) differs considerably between

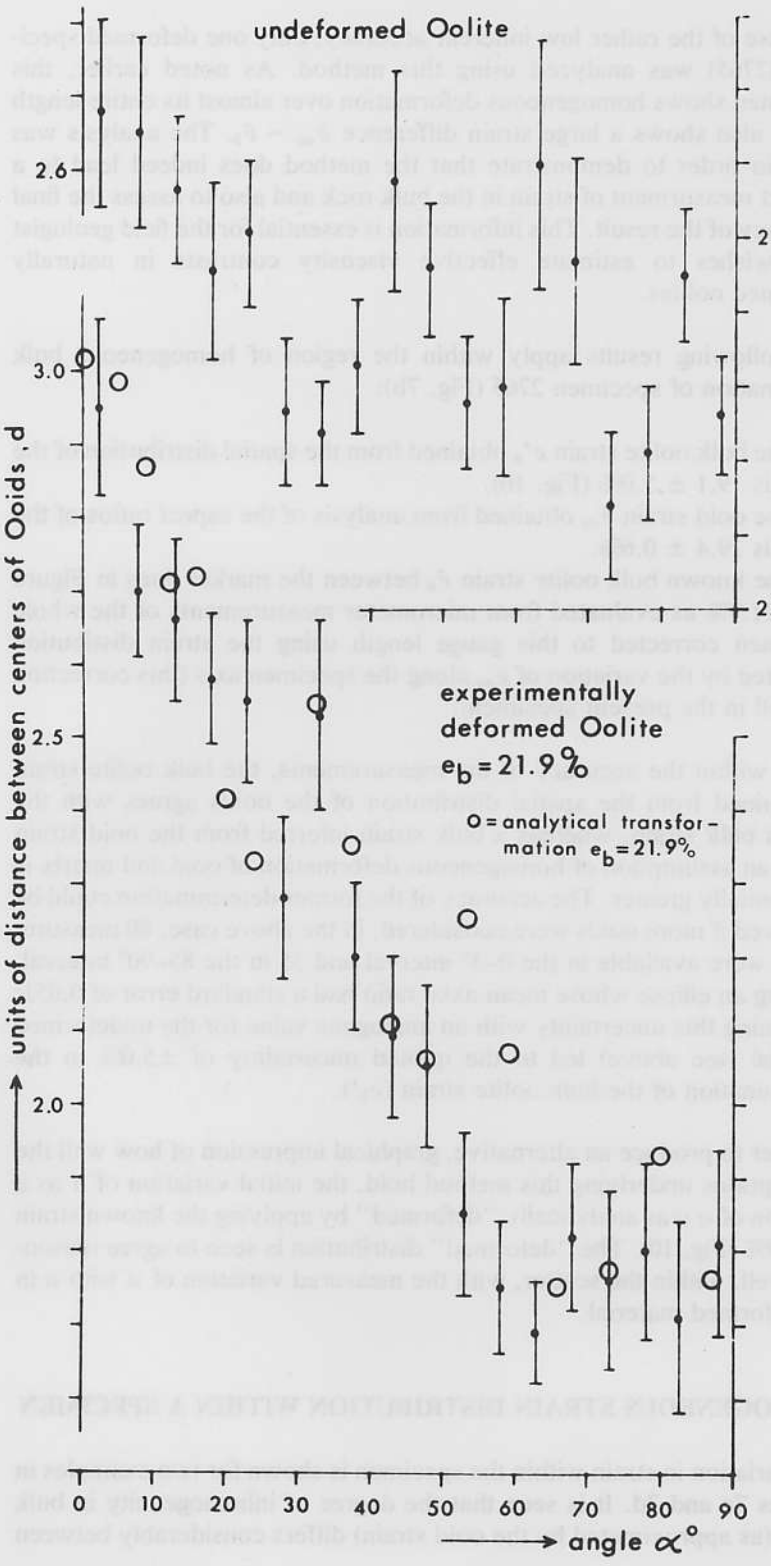
undeformed Oolite
2.6
2.5
3.0
2.0
experimentally
deformed Oolite
$e_b = 21.9\%$
O = analytical transfor-
mation $e_b = 21.9\%$
units of distance between centers of Ooids, d
2.5
2.0
0
10
20
30
40
50
60
70
80
90
angle $\alpha°$

the two samples deformed under different conditions. In general, the degree of inhomogeneity is greater when the deformation involves higher stresses. The same effect has been observed in Solenhofen limestone, where barreling is absent over most of the specimen length in low stress experiments (that is, with differential stresses of a few hundreds or tens of bars).

The inhomogeneity of deformation expressed in the barreling of a compression specimen can be attributed to the influence of the constraint imposed on deformation near the ends of the specimen due to friction between the loading piston and the specimen. This constraint leads to there being adjacent to the endface a roughly conically shaped region in which the deformation is relatively small. The barreling then arises from the distribution of lateral displacement during shortening as these conical regions approach each other. It is proposed here that the degree of barreling in specimens deformed under different conditions is related to the different degree of stress dependence of the strain rate, as measured by the parameter n if the power law holds.

Under conditions where the flow stress is relatively high, n is high (Fig. 4) and, therefore, the strain rate is relatively strongly sensitive to differences in stress. Such differences in stress within the specimen are imposed by the frictional constraints exerted by the pistons on the endfaces of the specimen. In the center of the specimen the deviatoric stress causing flow is given by the stress difference between axial stress and confining pressure. Near the pistons, the additional stress components arising from the frictional constraint have the qualitative effect of increasing the confining pressure and so reducing the deviatoric stress near the piston. Taking the amount of change in deviatoric stress between the end and the center of the specimen as being always the same, it can then be seen that the total variation in strain rate between end and center will be greater the more stress sensitive is the strain rate, that is, the higher is the value of n. Thus, the material having higher n will develop a greater degree of inhomogeneity of strain, expressed as the difference in relative shortening in the axial direction between center and end of the specimen, and hence in the barreling.

Fig. 10. Plot of the length d of the line joining neighboring ooids versus α, its angle to the bedding plane *(top diagram)* or the direction normal to the specimen axis *(bottom diagram). Top diagram* applies to a typical specimen before deformation; *Bottom diagram* applies to specimen 2765 within the region of homogeneous bulk strain. *Closed symbols* and *bars:* arithmetic mean and standard error of groups of measurements within 5° intervals in α. The variation after an analytical "deformation" corresponding to the known 21.9% shortening is shown by the open symbols

8 COMPARISON WITH THEORY

Recently, Bilby et al. (1975) analytically treated the change of shape of a viscous oblate spheroid in a matrix of different viscosity, modifying and extending an earlier study by Gay (1968). Their Equation (17) (Bilby et al., 1975) describes the development of strain in the spheroid parallel to its short axis as a function of the strain remote from the inclusion and of the viscosity contrast, r, defined as the ratio of the viscosity in the inclusion to the viscosity in the surrounding material. Newtonian viscosity is assumed.

The model of Bilby et al. (1975) clearly cannot be used to represent in all respects the oolite studied here because the model considers only a single inclusion within a surrounding material of a homogeneous but different viscosity. In the case of the oolite, the ooids form a multiplicity of inclusions which are closely spaced and interact, that is, the perturbation in an otherwise homogeneous strain field due to the presence of a given ooid overlaps the perturbations due to neighboring ooids. The flow resistance of the coarser-grained matrix, which itself might be represented by that of Carrara marble, is relevant only immediately adjacent to the ooid boundary, while in respect of interaction over longer distances the ooid will behave as if it were immersed in a medium having the properties of the bulk oolite. Therefore, in selecting data for comparing the model of Bilby et al. (1975) with the oolite, the flow stress of the bulk oolite is taken as determining the viscosity of the surrounding medium. To obtain a viscosity for the inclusion itself, we have tentatively used the flow stress of Solenhofen limestone on account of its fine grain size and characteristic flow behavior described above. Another difficulty in applying the model to the present situation lies in the non-Newtonian behavior of the materials of the oolite but we at first overlook this difficulty and return to it later.

The behavior of the model of Bilby et al. has therefore been calculated for viscosity ratios r equal to the ratios of the flow stresses of Solenhofen limestone and the bulk oolite at the relevant temperatures and strain rates (Table 2) and plotted on Figure 8 for comparison with our results. At 900°C, 10^{-5}/s strain rate ($r = 0.34$) excellent agreement is shown. However, at 800°C, 10^{-5}/s ($r = 0.88$), the ooids undergo relatively more strain than would be predicted by the theory; and at 700°C, 10^{-3}/s ($r = 1.37$), the ooids are still undergoing more strain than the average rock even though the theory now predicts less inclusion strain because the viscosity ratio is now greater than unity. Since it seems unlikely that taking into proper account the influence of the non-Newtonian nature of the effective viscosities would change the qualitative significance of a change of viscosity ratio from greater than unity to less than unity, we conclude that the discrepancy between observed and the predicted

relative strains lies in the choice of Solenhofen limestone as a model material for the ooids. This conclusion is reinforced by the observation above that at 700°C the oolite is, in fact, weaker than both Carrara marble and Solenhofen limestone (Table 2). Thus, in the 700° and 800°C cases the ooid material must be assumed to be substantially weaker than Solenhofen limestone in spite of the similarity in grainsize, suggesting that differences in impurity content may be significantly affecting the relative strengths. The question then arises as to why the 900°C behavior does not show a corresponding discrepancy with the theory. Possibly the biasing factors affecting the 700° and 800°C behavior are counterbalanced by the effect of the reversed grain size differential that is now more marked due to the extra grain-growth in the ooids at 900°C (Table 2). But it must also be noted that the comparison with theory is less sensitive to variations in viscosity ratio as the latter approaches zero, and it is also possible that the departure from Newtonian viscosity becomes more significant then, too. Unfortunately, it is not possible to assess from the present work the role played by the non-Newtonian nature of the viscosity, except to speculate that it gives rise to what appears to be a somewhat greater curvature in the observed trends in Figure 8 than is predicted by the Newtonian theory; however, this curvature may have another explanation.

9 GEOLOGICAL APPLICATIONS

The scope and accuracy of strain determinations using deformed, originally quasi-spherical objects has been greatly improved by taking into account both the axial ratios and the orientations of the originally ellipsoidal strain markers (Elliott, 1970). However, apart from theoretical studies (Gay, 1968; Bilby et al., 1975), not much progress has been made in evaluating the other main source of errors in the strain determination in rocks, namely the contrast in flow behavior between strain marker and matrix. The present study concerns this second source of error only. Because of the inhomogeneous strain distribution within the test specimens a direct test on more sophisticated methods of strain determination, such as the one described by Elliott (1970) and primarily concerned with eliminating errors arising from the initial shape and orientation of strain markers, could not be made.

Our results indicate that the determination of bulk strain in naturally deformed oolites from the shape of the ooids may involve substantial error if the conditions of deformation are equivalent to those in the higher temperature experiments, whereas such a strain analysis may be reliable if the conditions are equivalent to those in the lower temperature experiments. Which circumstances applies most generally in practice can only be determined directly by the study of situations in the field in

which an independent determination of the bulk strain can be made on other bases. (In Sect. 6.2 such an alternative strain analysis was demonstrated to indicate bulk strain in the oolite.) However, there are some pointers to the existence of a strong grain-size dependence in monomineralic calcite rocks and therefore to the likelihood of heterogeneity of deformation between coarse and fine-grained parts of rocks, for example, in oolites. Such fossils as belemnites (coarse grained) and crinoid stems (single crystals), embedded in a matrix of fine-grained limestone, are often disrupted and internally hardly deformed at all (Ramsay, 1967) while foliation or the flattening of ooids indicates high amounts of strain. Such observations would indicate that the high temperature runs are more representative for the geological environment and that viscosity contrasts would occur in an oolite such as the one listed in this study.

Such a conclusion can also be drawn from a more theoretical approach. It has been pointed out earlier (Sect. 5) that the effective viscosity contrast at high temperatures in this oolite probably results from a transition to a deformation mechanism of diffusional flow and/or grain boundary sliding in the finegrained ooids. These deformation mechanisms are grain size dependent, a small grain size favoring faster strain rates at any given stress. A relationship of the form $\epsilon \propto 1/L^a$, where L is the grain size and where $1 < a < 3$, fits most materials behaving superplastically (Edington et al., 1976) and is predicted by models of diffusional flow (Stocker and Ashby, 1973). So the question of the likelihood of such viscosity contrasts in oolites is reduced to the question whether grain size sensitive deformation mechanisms such as the ones mentioned above occur in nature or not. When fields of deformation mechanisms are plotted in the form of deformation mechanism maps (Stocker and Ashby, 1973) in stress–temperature space, it becomes evident that the transition from one deformation mechanism into another is primarily a function of differential stress. In this light it seems likely that the high temperature runs, where "geologically realistic" flow stresses are believed to have been achieved, are the ones representative of many crustal environments.

Viscosity contrasts inferred to have given rise to strain heterogeneity between marker inclusions and the bulk rock can be conversely used as evidence revealing the stress regime of the natural deformation, and hence its temperature–strain rate regime, if the strain heterogeneity can be independently established and if the factors determining the rheological behavior of the component materials of the rock have been well established. To exploit such a possibility is perhaps an ambitious and long-term aim but it is illustrative of one way in which coordination between field and laboratory studies may eventually further our understanding of the geological record.

ACKNOWLEDGMENTS

We wish to thank J. N. Boland, R. S. Coe and I. van der Molen (ANU) as well as W. Müller and O. A. Pfiffner (ETH Zürich) for many discussions and suggestions. W. Müller kindly provided the test material. The technical assistance by T. White (apparatus) and P. Willis (thin sections) is also acknowledged.

REFERENCES

Bilby, B. A., Eshelby, J. D., Kundu, A. K.: The change of shape of a viscous ellipsoidal region embedded in a slowly deforming matrix having a different viscosity. Tectonophysics *28*, 265–274 (1975)

Cloos, E.: Oolite deformation in the South Mountain fold, Maryland. Geol. Soc. Am. Bull. *68*, 843–918 (1947)

Davies, G. J., Edington, J. W., Cutler, C. P., Padmanabhan, K. A.: Superplasticity: A Review. J. Mat. Sci. *5*, 1091–1102 (1970)

Edington, J.W., Melton, K. N., Cutler, C. P.: Superplasticity. Progr. Mat. Sci. *21*, 61–158 (1976)

Elliott, D.: Determination of finite strain and initial shape from deformed elliptical objects. Geol. Soc. Am. Bull. *81*, 2221–2236 (1970)

Gay, N. C.: Pure-shear and simple-shear deformation of inhomogeneous viscous fluids. 1. Theory. Tectonophysics *5*, 211–234 (1968)

Heard, H. C., Raleigh, C. B.: Steady-state flow in marble at 500–800°C. Geol. Soc. Am. Bull. *83*, 935–956 (1972)

Kohlstedt, D. L., Goetze, C., Durham, W. B.: Experimental deformation of single crystal olivine with application to flow in the mantle. In: Petrophysics: The Physics and Chemistry of Minerals and Rocks. Runcorn, S. K. (ed.) London: John Wiley and Sons, (in press)

Paterson, M. S.: A high-pressure high-temperature apparatus for rock deformation. Intern. J. Rock Mech. Min. Sci. *7*, 517–526 (1970)

Paterson, M. S.: Some current aspects of experimental rock deformation. Phil. Trans. R. Soc. London Ser. A. 208, 163–171 (1976)

Ramsay, J. G.: Folding and Fracturing of Rocks. New York: McGraw-Hill, 1967, 567 pp.

Schmid, S. M.: Rheological evidence for changes in the deformation mechanism of Solenhofen limestone towards low stresses. Tectonophysics *31*, T21–T28 (1976)

Stocker, R. L., Ashby, M. F.: On the rheology of the upper mantle. Rev. of Geophys. Space Phys. *11*, 391–426 (1973)

Tan, B. K.: Deformation of particles developed around rigid and deformable nuclei. Tectonophysics *24*, 243–257 (1974)